J Mater Sci (2009) 44:414–421
DOI 10.1007/s10853-008-3143-7

Compaction of different boron carbide powders using uniaxial die compaction and combustion driven compaction

Xiaojing Zhu · Kathy Lu · Karthik Nagarathnam

Received: 5 August 2008 / Accepted: 26 November 2008 / Published online: 11 December 2008

Abstract Compaction of pure B_4C and Ni_2B nanolayer coated B_4C was studied using uniaxial die compaction and combustion driven compaction techniques. Effects of different compaction techniques and the Ni_2B nanolayer around B_4C particle surfaces on green B_4C sample characteristics are the focus of this study. The combustion driven compaction process yields much higher green density and strength than the uniaxial die compaction process. For the samples obtained from the same compaction technique, the Ni_2B nanolayer on individual B_4C particle surfaces improves the green density and strength of the B_4C powder compacts. For the combustion driven compaction process, optical images show micro-cracks on the surface of pure B_4C compact while crack-free surface is observed for Ni_2B nanolayer coated B_4C sample. Scanning electron microscopy analysis shows the same trend as the green density and strength measurements. Combustion driven compaction diagram for hard and brittle materials such as B_4C is discussed.

Introduction

B_4C has high melting point (2,450 °C), high hardness (2,900–3,580 Knoop), good chemical resistance, low density (2.52 g/cm^3), and desirable neutron absorption capabilities [1]. These characteristics make B_4C an important material in different applications. B_4C can be used for dressing diamond tools, hot-pressed shot blast nozzles, ceramic tooling dies, and armors. B_4C is also used as an absorbent for neutron radiation in nuclear power plants in the form of shielding, control rod, and shut down pellets. However, the high melting point and high hardness make B_4C very difficult to process and intrinsically brittle. Hot-pressing can produce high density B_4C compacts but is expensive and has low efficiency [2, 3]. Innovative techniques are highly desired for flexible, low cost, and high efficiency B_4C processing. To meet such requirement, the first step is to explore new method of forming B_4C compacts.

Up to now, B_4C has been mostly compacted using uniaxial die compaction technique. In order to increase the green density and facilitate the sintering densification, additives are widely used. However, incorporation of additives, such as TiB_2 and SiC, showed limited incremental improvement [4, 5]. B_4C, TiO_2, and carbon mixture was cold-isostatic compacted at 300 MPa [6]. The TiO_2 content was changed from 9.23 to 32.97 wt%. However, the green density of the compacts was only 67–75%. B_4C and carbon mixture green samples were made by uniaxial die compaction at 200 MPa [7]. For the B_4C-carbon mixture with 3 wt% of carbon, a green density of $\sim$70% was obtained. Mixtures of TiB_2, ZrO_2, carbon, and B_4C were compacted using uniaxial die compaction at 280 MPa [8]. A green density of $\sim$65% was obtained. As seen, the common issue for uniaxial die compaction of B_4C-containing powder is the low green density obtained. If pure B_4C is to be compacted, much lower green density can be expected.

Two approaches can be considered to address this problem. One is using high pressure compaction and the other is modifying B_4C powder in a more effective manner.

X. Zhu · K. Lu (✉)
Department of Materials Science and Engineering, Virginia Polytechnic Institute and State University, 213 Holden Hall-M/C 0237, Blacksburg, VA 24061, USA
e-mail: klu@vt.edu

K. Nagarathnam
Utron, Inc., Manassas, VA, USA

Several different high pressure compaction techniques have emerged in the recent years with the aim to improve the green density of hard-to-compact materials, such as B_4C. Among these are the conventional compaction by pushing the limit of existing presses, diamond anvil compaction, plasma pressure compaction, dynamic compaction, and shock wave compaction [9–15]. However, it is difficult to achieve greater than 1 GPa compaction pressure for conventional compaction process to fulfill the needs of B_4C compaction; diamond anvil compaction requires special deformable dies and complicated compaction procedures; other techniques require either complex equipment or electrical and magnetic field. For example, shock wave compaction uses high velocity compressive waves and almost always creates micro-cracks in the produced articles [16].

Combustion driven compaction (CDC) is a unique technique developed by Utron Inc. [17–19]. The high pressure generated from a combustion gas mixture (methane and air) compacts the powder of interest with a simple set up and no requirement of specific field such as electrical field or magnetic field. During compaction, the sealed gas mixture is ignited; and the pressure in the chamber rises dramatically in a very short period of time. At the same time, the top ram is pushed down on the powder at an extremely high speed, realizing the compaction. This technique has been very effective for metallic powder compaction. Sm–Co and Fe nanostructured magnets were prepared using the CDC technique [20] and coercivity loss was greatly reduced. Different green parts with complex shapes including rings, dogbones, cylinders, and gears were prepared at greater than 2.0 GPa pressure [17]. About 98% green density has been achieved for Al-3 Mg alloy particles, 97.85% green density for copper particles, and 97% green density for stainless steel particles [21]. Based on these results, the CDC process appears to be a promising technique for the compaction of B_4C powders.

From a different prospective, if a thin and compliant layer can be applied onto B_4C particle surfaces, it should greatly facilitate the rearrangement of the B_4C particles during compaction. When the amount of the compliant layer is controlled at a very low level and distributed homogeneously on the B_4C particle surfaces, such as in nanolayer format, it should not cause significant performance degradation, thus making B_4C processing more flexible. Nickel is one of the metals that have been studied and used extensively in coatings because of its unique properties such as good ductility, lubricity and excellent corrosion, and wear resistance. If nickel can be applied onto B_4C particle surfaces uniformly in the form of a thin layer, it presents great potential to improve the processability of B_4C powder.

In this study, CDC and uniaxial die compaction techniques are compared in their abilities of forming B_4C compacts. Two different B_4C powders, pure B_4C, and Ni_2B nanolayer coated B_4C, are used in order to evaluate the effect of the Ni_2B compliant nanolayer on B_4C particle surfaces. Green densities, green strengths, and microstructures of the B_4C compacts obtained from the two compaction techniques and two different B_4C powders are examined. The effects of the Ni_2B nanolayer on B_4C particle compaction are evaluated and three compaction stages for the CDC process are discussed.

Experimental procedure

The pure B_4C powder (H. C. Starck, Inc., Newton, MA) used had 2.27 μm average particle size (Horiba, LA-950, Irvine, CA). There were some small, satellite B_4C particles attached onto the larger size B_4C particle surfaces (Fig. 1a). The method of producing Ni–B nanolayer onto B_4C particles by electroless coating was reported before [22, 23]. The as-coated Ni–B nanolayer on the B_4C particle surfaces had a mesh-like structure and was 50–70 nm thick. Ni–B nodules were randomly embedded in the mesh structure. Ni:B elemental ratio was 2.5:1 for the nanolayer. Before compaction, the Ni–B nanolayer coated B_4C powder was thermally treated in an $Ar–H_2$ atmosphere to remove the accompanying Ni_2O_3 and B_2O_3 in the nanolayer [24]. At 800 °C, the Ni–B nanolayer evolved into Ni_2B. The Ni_2B nanolayer on the B_4C particle surfaces had around 50 nm thickness but some particle-like features were present (Fig. 1b). The cross section scanning electron microscopy (SEM) image of the Ni_2B nanolayer coated B_4C powder was obtained by focused ion beam cross-sectioning (FEI Helios 600 NanoLab, Hillsboro, OR) as shown in Fig. 1c. As seen, the dark B_4C particles were surrounded by the bright Ni_2B nanolayer.

Uniaxial die compaction was used to compact the pure B_4C and Ni_2B nanolayer coated B_4C powders (TMS 810 Material Test System, MTS Systems Corporation, Eden Prairie, MN). Compaction was carried out with a load application rate of 10 MPa/s and a load release rate of 2 MPa/s. The load was held at peak pressure for 120 s. For the pure B_4C powder, the peak pressure was 180 MPa. For the Ni_2B nanolayer coated B_4C powder, the peak pressure was 200 MPa. The diameter of the compacts was 25.07 mm. Since similar amounts of B_4C powders were used for die filling, the thicknesses of the compacts were close, around 2.20 and 1.92 mm for the pure and the Ni_2B nanolayer coated B_4C samples, respectively.

The above two powders were also compacted by the CDC technique (300-Ton Model, Utron, Inc., Manassas, VA). The compaction process was carried out with 2.02 GPa peak pressure. The diameter of the compacts was 25.70 mm. The thickness of the compacts was 1.83 and

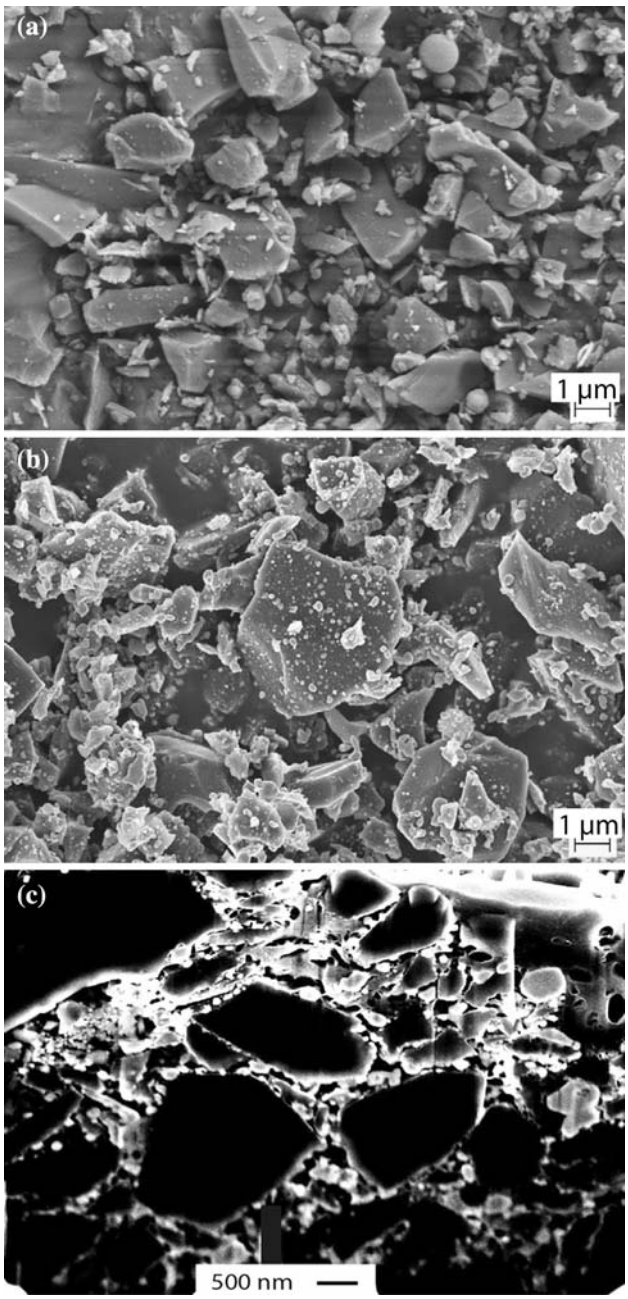

Fig. 1 SEM images showing particle surface morphology of: **a** pure B_4C, **b** Ni_2B nanolayer coated B_4C at as-is condition, and **c** cross-sectioned Ni_2B nanolayer coated B_4C

1.40 mm for the pure B_4C and the Ni_2B nanolayer coated B_4C samples, respectively, with similar amounts of B_4C powders used in die filling.

Green densities were obtained by measuring the dimensions and weights of the samples. Equibiaxial flexural strength (abbreviated as green strength) of the B_4C powder compacts was determined following ASTM C 1499 [25]. The samples were tested using a texture analyzer test console equipped with a 5 kN load cell (Stable Micro Systems, Surrey, UK). The console was set to record compressive forces and the crosshead was lowered monotonically at a speed of 0.1 mm/s. The peak force at which the compact broke was recorded [26]. The green strength was calculated using Eq. 1 [26]

$$\sigma_f = \frac{3F}{2\pi h^2}\left[(1-v)\frac{D_S^2 - D_L^2}{2D^2} + (1+v)\ln\frac{D_S}{D_L}\right] \quad (1)$$

where σ_f is fracture strength in unit of MPa, F is breaking force in unit of N, h is specimen thickness in unit of mm, v is Poisson's ratio, D is sample diameter in mm, D_S is the diameter of the supporting ring in mm, and D_L is the diameter of the loading ring in mm. In this study, v was assumed to be 0.2 for the brittle B_4C green samples. D_s was 22.225 mm. D_L was 12.7 mm. D and h values were as given before.

An optical microscope was used to examine the B_4C compact surfaces (KH-7700, Hirox Company, River Edge, NJ). A field emission SEM (LEO 1550, Carl Zeiss MicroImaging, Inc., Thornwood, NY) was used to examine the fracture surfaces of the B_4C compacts.

Results and discussion

Green density

Table 1 shows the green densities of the B_4C samples made by the uniaxial die compaction and CDC techniques. Each value is an average of the densities from four different samples. For the pure B_4C compacts, 2.52 g/cm^3 is taken as the theoretical density for the density calculation in Table 1. For the samples made from the Ni_2B nanolayer coated B_4C powder, 3.01 g/cm^3 is used as the theoretical density, calculated based on the previous XRD data [24]. Even though this latter value overestimates the theoretical density and it underestimates the relative densities of the Ni_2B nanolayer coated B_4C powder without considering the nickel loss during the electroless coating process, it can sufficiently identify the impact of the Ni_2B layer without introducing other density measurement errors. Even with this, the green densities show clear beneficial impacts from the Ni_2B nanolayer and the CDC technique. For the uniaxial die compaction process, the average density is 55.3% for the pure B_4C samples and 53.8% for the Ni_2B nanolayer coated B_4C compacts; and the standard deviation is 0.01 for both samples. For the CDC technique, the average density is 64.9% for the pure B_4C samples and 73.3% for the Ni_2B nanolayer coated B_4C compacts; and the standard deviation is 0.002 and 0.003 for the two corresponding kinds of samples, respectively.

For the uniaxial die compaction technique, there is no clear relative density difference. However, it is very

Table 1 Green density of B_4C compacts made by uniaxial die compaction and CDC

Sample	Uniaxial die compaction		CDC	
	Absolute density, g/cm^3	Relative density, %	Absolute density, g/cm^3	Relative density, %
B_4C	1.39 ± 0.03	55.3 ± 0.01	1.63 ± 0.006	64.9 ± 0.002
Ni_2B nanolayer coated B_4C	1.62 ± 0.04	53.8 ± 0.01	2.21 ± 0.008	73.3 ± 0.003

difficult to compact the pure B_4C powders; and the B_4C particles do not hold together until a few drops of ethanol are added. Otherwise, severe sample cracking occurs and then leads to complete compact fracture. The Ni_2B nanolayer coated B_4C powder can be compacted more easily with the uniaxial die compaction method. The pure B_4C compacts have a slightly higher relative density than the Ni_2B nanolayer coated B_4C compacts but the density difference is only about 1.5%. The slightly higher density from the pure B_4C compacts could be attributed by the addition of ethanol which facilitates B_4C particle rearrangement. Also, as pointed out, the relative density calculation for the Ni_2B nanolayer coated B_4C sample overestimates the nickel amount in the Ni_2B nanolayer and underestimates the Ni_2B nanolayer coated B_4C compact relative density. More importantly, the uniaxial die compaction pressure is low and the pure B_4C and the Ni_2B nanolayer coated B_4C powders are in the early stage of compaction. The Ni_2B nanolayer has not started to play a significant role in the B_4C powder compaction yet.

The B_4C compacts from the CDC technique have much higher green density than those from the uniaxial die compaction, with the Ni_2B coated B_4C sample showing much larger relative density difference (73.3% vs. 53.8%). This demonstrates the advantage of the CDC technique over the uniaxial die compaction process in obtaining high green density samples. For the B_4C powder, the high green density of 73.3% has not been achieved before without introducing a substantial amount of secondary additive(s). Also, comparing the two green densities from the CDC technique, the density of the Ni_2B nanolayer coated B_4C compact is much higher than that of the pure B_4C compacts (73.3% vs. 64.9%). This result indicates that the Ni_2B nanolayer can effectively improve the compaction of the B_4C powder. The above observation is consistent with the discrete element modeling results, which show that hard particles result in a stiffer response to the compaction pressure because of the lack of sliding and rearrangement between particles and deformation of particles themselves [27].

Green strength

For the uniaxial die compacted samples, the breaking force for the pure and the Ni_2B nanolayer coated B_4C samples was 1.75 N and 8.65 N, respectively. For the combustion driven compacted samples, the breaking force for the pure and the Ni_2B nanolayer coated B_4C samples was 2.2 N and 51.2 N, respectively. Based on these measurements, Table 2 shows the green strengths and the standard deviation for the pure B_4C and the Ni_2B nanolayer coated B_4C compacts from the uniaxial die compaction and the CDC techniques. For the same compaction technique, there is a large difference in the green strength between the two different kinds of B_4C powder compacts. The pure B_4C compacts show lower green strength: 0.15 MPa for the uniaxial die compacted samples and 0.27 MPa for the combustion driven compacted samples. The Ni_2B coated B_4C compacts show much higher green strength: 0.99 MPa for the uniaxial die compacted samples and 10.90 MPa for the combustion driven compacted samples. Also, the CDC technique produces much higher green strength samples than the uniaxial die compaction process, generally 2–10 times higher.

The improved green strength for the Ni_2B coated B_4C compacts from both compaction techniques is attributed by the presence of the Ni_2B nanolayer. During the compaction, the Ni_2B nanolayer acts as a lubricant between B_4C particles, reduces the friction between B_4C particles, and leads to easier B_4C particle sliding and rearrangement. Also, the compliant Ni_2B nanolayer is believed to provide more bonding between the B_4C particles. Hence, B_4C particles pack more efficiently, giving a much higher green strength compared to the pure B_4C powder compacts. The

Table 2 Green strength of pure and Ni_2B coated B_4C powder compacts

Sample	Uniaxial die compaction		CDC	
	Green strength, σ_f, MPa	Standard deviation	Green strength, σ_f, MPa	Standard deviation
B_4C	0.15	0.01	0.27	0.05
Ni_2B nanolayer coated B_4C	0.99	0.02	10.90	0.30

higher green strength of the CDC samples over the uniaxial die compacted samples originates from the nature of the CDC technique. During the CDC process, a much higher pressure (~2.02 GPa vs. 200 MPa) is imposed on the B_4C powder, which overcomes the friction between B_4C particles and forces them to pack more densely. The above features make the CDC process a more effective compaction technique.

Microstructure

The pure B_4C and Ni_2B coated B_4C powders respond differently to the CDC process. Figure 2 shows the optical images of the compact surfaces obtained by the CDC technique for each powder. As seen, there are visible micro-cracks on the surface of pure B_4C samples (Fig. 2a). On the other hand, there are hardly any micro-cracks seen on the Ni_2B nanolayer coated B_4C sample surface (Fig. 2b).

For the pure B_4C compact undergoing the CDC process, the pressure propagation surface inside the B_4C compact can be envisioned as consisting of a loading front, followed by a region of high amplitude pressure. The front is believed to span a thickness of 1–100 μm, its irregularity caused by competition between rapid loading of particles and unloading from voids that are yet to collapse [28, 29]. In some locations, the localized, intensive pressure on the contact surfaces keeps increasing without involving adjacent particle contacts [28]. The local pressure distribution in the B_4C compact can vary by as much as a few GPa. B_4C particles have high hardness and do not deform even under such extremely high local pressures. Also, B_4C particles have irregular shapes and cannot slide over each other easily during compaction. The pure B_4C compact most likely has a strongly anisotropic network of heavily stressed contacts. Pressure variations of such magnitude following the loading front cannot be represented by the applied pressure, which instead indicates an averaged measure of the B_4C compact response. Also, the irregular B_4C particle shapes prevent the particles from swiftly returning to the mechanism equilibrium. These factors in combinations lead to high stress concentrations and a considerable amount of micro-cracks in the B_4C compact. This stress anisotropy and the micro-cracks created during the fast pressure increase stage cannot be sufficiently eliminated by the slower pressure release stage during the CDC process.

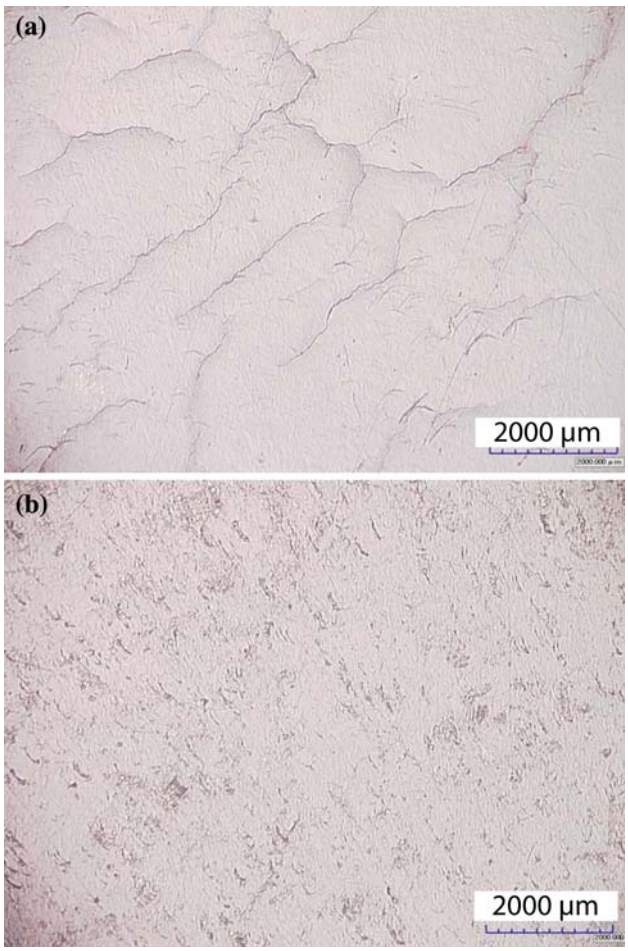

Fig. 2 Optical images of B_4C compact surfaces from CDC process: **a** pure B_4C powder, and **b** Ni_2B nanolayer coated B_4C powder

For the Ni_2B nanolayer coated B_4C compact, the distribution of normal contact forces are believed to fall into two categories—the 'weak force chains' and 'strong force chains.' The weak force chains are comprised of contacts that carry less than average contact force, and the strong force chains carry a greater than average force. Sliding occurs predominantly within the weak force chains, and in this case, it occurs along the Ni_2B nanolayer boundaries. The contacts in the strong force chains make the dominant contribution to the stress concentration [30] but the corresponding magnitude is not as high as that of the pure B_4C compact. Compact cracking does not occur for the Ni_2B nanolayer coated B_4C powder. This result implies that the Ni_2B nanolayer can not only enhance the compaction of the B_4C particles but also act as a bonding layer to modulate the internal stress distribution. The particle rearrangement and bonding, even under the applied high velocity and high magnitude pressure, lead to more homogeneous compaction pressure distribution. This in turn effectively avoids micro-cracks. The Ni_2B nanolayer also increases the adhesion between the B_4C particles and offers higher green strength as seen in Table 2.

Since the pure B_4C samples from the uniaxial die compaction process have low green strength and are very fragile, no fracture surface can be successfully prepared for the SEM analysis. As a result, Fig. 3 only shows the fracture surfaces of the Ni_2B coated B_4C compacts made

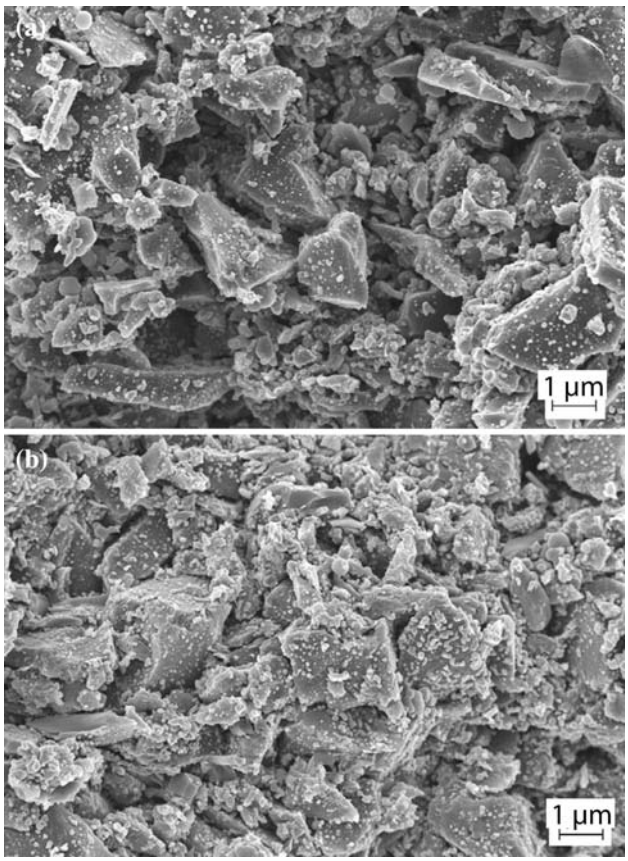

Fig. 3 SEM images of fracture surfaces of Ni_2B coated B_4C compacts made by **a** uniaxial die compaction, and **b** CDC

by the uniaxial die compaction (Fig. 3a) and CDC processes (Fig. 3b). Consistent with the green density and strength measurements, the B_4C compacts made by the CDC technique show denser B_4C particle packing (Fig. 3b), which can be explained by the 10 times higher compaction pressure used in the CDC process. This result confirms the effectiveness of the CDC process in providing higher green density samples without using high content of secondary additive(s). In Fig. 3, it can be seen that the Ni_2B nanolayer remains intact for both the compaction techniques, demonstrating the effectiveness of the Ni_2B nanolayer.

In order to compare powder effect on the compaction process, the fracture surface of the pure B_4C compacts made by the CDC technique is shown in Fig. 4. There is no particle deformation even under 2.02 GPa compaction pressure because of the high B_4C hardness. Also, there is little B_4C particle rearrangement. A closer examination shows that a few particles fracture into two pieces, as indicated in the ovals. This is because during the CDC compaction process, there are not many small particles to fill the interstitial sites between large B_4C particles. As a result, the effective pressure on individual B_4C particles is

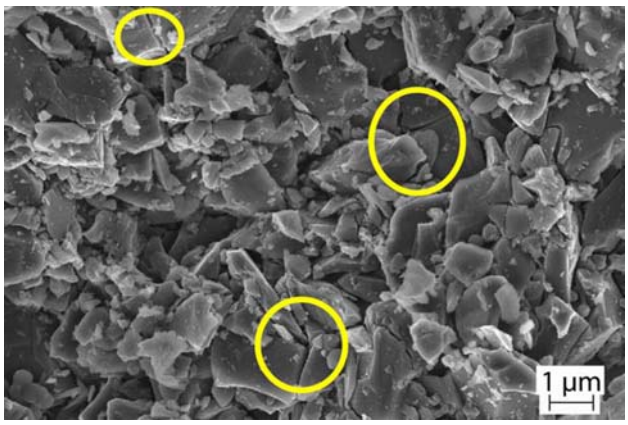

Fig. 4 SEM image of fracture surface of pure B_4C compact made by CDC

high. This extremely high effective pressure at localized regions leads to cracks seen in Fig. 4. In contrast, the Ni_2B nanolayer coated B_4C powder compact shows dense packing, as seen in Fig. 3b. There is no individual B_4C particle cracking observed.

CDC compaction stages

Based on the above discussion and understanding, the compaction diagram of the CDC process can be described as follows (Fig. 5): pre-compaction stage, compaction stage, and pressure release stage. During the pre-compaction stage (within the first 100 ms), a combustion gas (such as methane) and air create a pre-pressure pushing the upper ram down, pre-compacting the particles, and removing the entrapped air among the particles. During the compaction stage (reaching peak pressure within 250 ms), an ignition stimulus is applied causing combustion in the gas chamber. The gas mixture generates extremely high pressure (>2 GPa) within a fraction of a second. This pressure

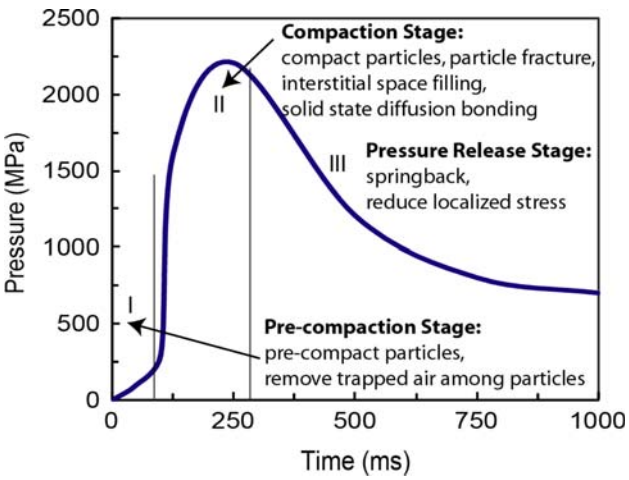

Fig. 5 CDC compaction diagram

increase compacts the particles to a high green density in a very short time but in a locally inhomogeneous manner. Depending on the compositions, the distribution of the corresponding species, and the morphology of the corresponding species, particles might fracture and fill the interstitial sites, and solid state diffusion bonding might occur [30, 31]. For the particle system with thin and compliant surface layers, the high force network can be modulated and the stress concentration can be lowered. During the pressure release stage (>750 ms), some springback gradually occurs to release the compact internal stress. This slow pressure release process can reduce the sample cracking possibility to a certain extent. The end result is a high density compact within a couple of minutes for properly designed powder(s). Compared to other high pressure compaction techniques, the CDC process imposes pressure at a much gentler manner during its unique three-stage cycle, making it very attractive for brittle, crack-sensitive materials.

The function of the Ni_2B nanolayer during and after the CDC compaction process can be understood as follows. First, the Ni_2B nanolayer acts as a 'lubricating layer' to reduce the interparticle frictional force and facilitate B_4C particle sliding and rearrangement with respect to each other under the compaction pressure, which is rarely possible for the pure B_4C powder. Second, the Ni_2B nanolayer improves the green strength and avoids micro-cracking of the Ni_2B coated B_4C sample by offering stronger bonding between the B_4C particles. The rearrangement, high velocity impact, and localized heating and welding of the Ni_2B nanolayer coated B_4C particle surfaces play important roles in the high green density and crack-free B_4C compact formation. The stress concentration at the B_4C particle–particle contacts is effectively alleviated by the ductile deformation of the Ni_2B nanolayer. The combination of greater than 2 GPa compaction pressure and the lubricating Ni_2B layer produces a unique opportunity for highly effective B_4C compaction.

After the combustion driven compaction, a continuous Ni_2B network forms in the B_4C compact. The uniform distribution of the Ni_2B nanolayer strongly holds the B_4C particles together and prevents defect formation while allowing stress release. This leads to much stronger B_4C samples with high green strength, making the CDC process especially attractive for highly brittle materials that have to endure many handling processes before being sintered.

Conclusions

In this work, compaction of pure B_4C and Ni_2B nanolayer coated B_4C powders was carried out using uniaxial die compaction and combustion driven compaction techniques. The effects of the Ni_2B nanolayer on the compaction of the B_4C powder for both techniques were evaluated. The CDC process yields much higher green density and strength for both B_4C powders than the uniaxial die compaction technique. For the compacts obtained from the same technique, the Ni_2B nanolayer coated B_4C compact yields higher green density and strength. The pure B_4C powder compact from the CDC technique has surface micro-cracks. The Ni_2B coated B_4C compact from the CDC technique is crack-free. The CDC compaction diagram for hard, brittle materials like B_4C has been discussed.

Acknowledgement The authors acknowledge the financial support from National Science Foundation under grant No. DMI-0620621.

References

1. Schneider SJ (1991) Ceramics and glasses-engineering materials handbook. ASM International, Materials Park, OH
2. Zhao H, Hiragushi K, Mizota Y (2003) J Eur Ceram Soc 23:1485
3. Deng JX, Zhou J, Feng YH, Ding ZL (2002) Ceram Int 28(4):425
4. Zhen Y, Li A, Yin Y, Shi R, Liu Y (2004) Mater Res Bull 39:1615
5. Yamada S, Sakaguchi S, Hirao K, Yamauchi Y, Kanzaki S (2003) J Ceram Soc Jpn 111(1):53
6. Skorokhod VV, Krstic VD (2000) Powder Metall Metal Ceram 39(7–8):414
7. Lee H, Speyer RF (2003) J Am Ceram Soc 86(9):1468
8. Roy TK, Subramanian C, Suri AK (2006) Ceram Int 32(3):227
9. Gonzalez EJ, Hockey B, Piermarini GJ (1996) Mater Manuf Process 11(6):951
10. Gao L, Li W, Wang HZ, Zhou JX, Chao ZJ, Zai QZ (2001) J Eur Ceram Soc 21:135
11. Serdyuk GG, Sakhnenko AV, Svistun LI (2000) Powder Metall Metal Ceram 39(9–10):514
12. Raminga TP, van Zyl WE, Carton EP, Verweij H (2004) Ceram Int 30:629
13. Jaramillo D, Hinojosa G, Hallen JM, Balmori H, Inal OT (1997) Key Eng Mater 127(1–2):977
14. Venz GJ, Killen PD, Page NW (2003) J Mater Sci 38:2935. doi: 10.1023/A:1024417426146
15. Rabe T, Prummer R, Wasche R (1997) Mater Sci Forum 235–238(1–2):285
16. Sadangi RK, Shukla V, Kear BH (2005) Int J Refract Metal Hard Mater 23(4–6):363
17. Nagarathnam K, Trostle D, Kruczynski D, Maeesy D (2004) Proc Int Conf Powder Metall Part Mater. Chicago, IL, pp 1–15, 13–17 June 2004
18. Nagarathnam K, Renner A, Trostle D, Kruczynski D, Maeesy D (2007) Int Conf Powder Metall Part Mater. Denver, CO, 13–17 May 2007
19. Witherspoon FD, Massey DW, Mozhi TA, Kruczynski D, David L, Ryan JM (2004) Dynamic consolidation of powders using a pulsed energy source, Patent 6767505. Utron Inc
20. Sachan M, Majetich SA (2005) IEEE Trans Magn 41(10):3874
21. Kruczynski DL, Ryan JM, Trostle DS, Witherspoon FD, Massey DW (2002) Proc Int Conf Powder Metall Part Mater. Orlando, FL, 16–21 June 2002
22. Zhu XJ, Dong HY, Lu K (2008) Surf Coat Technol 202:2927

23. Dong HY, Zhu XJ, Lu K (2008) J Mater Sci 43:4247. doi: 10.1007/s10853-008-2615-0
24. Lu K, Zhu X, Thin Solid Films (submitted)
25. ASTM Designation C1499-04 in American Society for Testing and Materials International (2004) West Conshocken, PA, pp 767–777
26. Lu K (2008) J Mater Sci 43:652. doi:10.1007/s10853-007-2155-z
27. Skrinjar O, Larsson PL (2004) Acta Mater 52:1871
28. Benson DJ, Nesterenko VF, Jonsdottir F, Meyers MA (1997) J Mech Phys Solids 45:1955
29. Eakins DE, Thadhani NN (2008) Acta Mater 56:1496
30. Antony SJ, Kuhn MR, Barton DC, Bland R (2005) J Phys D 38:3944
31. Mamalis AG, Vottea IN, Manolakos DE (2001) J Mater Process Technol 108:165